AFGL-TR-87-0280

ESTIMATION OF SHORT-WAVELENGTH GRAVITY ON A DENSE GRID USING DIGITAL TERRAIN ELEVATION DATA

J.D. Goldstein
J.V. White
R.P. Corner
W.G. Heller

TMS ANALYTIC SCIENCES CORP.
55 Walkers Brook Drive
Reading, Ma 01867

October 1987

Scientific Report No. 1
May 1986 - May 1987

Prepared for:
AIR FORCE GEOPHYSICS LABORATORY
AIR FORCE SYSTEMS COMMAND
United States Air Force
Hanscom AFB, Massachusetts 01731

This technical report has been reviewed and is approved for publication.

VISHNU V. NEVREKAR
Contract Manager

THOMAS P. ROONEY, Chief
Geodesy & Gravity Branch

FOR THE COMMANDER

DONALD H. ECKHARDT, Director
Earth Sciences Division

This report has been reviewed by the ESD Public Affairs Office (PA) and is releasable to the National Technical Information Service (NTIS).

Qualified requestors may obtain additional copies from the Defense Technical Information Center. All others should apply to the National Technical Information Service.

If your address has changed, or if you wish to be removed from the mailing list, or if the addressee is no longer employed by your organization, please notify AFGL/DAA, Hanscom AFB, MA 01731-5000. This will assist us in maintaining a current mailing list.

Do not return copies of this report unless contractual obligations or notices on a specific document requires that it be returned.

UNCLASSIFIED

SECURITY CLASSIFICATION OF THIS PAGE

REPORT DOCUMENTATION PAGE

Form Approved
OMB No. 0704-0188
Exp. Date: Jun 30, 1986

1a. REPORT SECURITY CLASSIFICATION UNCLASSIFIED	1b. RESTRICTIVE MARKINGS NONE
2a. SECURITY CLASSIFICATION AUTHORITY N/A	3. DISTRIBUTION/AVAILABILITY OF REPORT Approved for Public Release; Distribution Unlimited
2b. DECLASSIFICATION/DOWNGRADING SCHEDULE N/A	
4. PERFORMING ORGANIZATION REPORT NUMBER(S) TR-5362-1	5. MONITORING ORGANIZATION REPORT NUMBER(S) AFGL-TR-87-0280
6a. NAME OF PERFORMING ORGANIZATION The Analytic Sciences Corp.	6b. OFFICE SYMBOL (If applicable)
6c. ADDRESS (City, State, and ZIP Code) 55 Walkers Brook Drive Reading, MA 01867	7a. NAME OF MONITORING ORGANIZATION Air Force Geophysics Laboratory
	7b. ADDRESS (City, State, and ZIP Code) Hanscom Air Force Base Massachusetts 01731
8a. NAME OF FUNDING/SPONSORING ORGANIZATION Defense Mapping Agency	8b. OFFICE SYMBOL (If applicable)
8c. ADDRESS (City, State, and ZIP Code) Washington, D.C. 20305	9. PROCUREMENT INSTRUMENT IDENTIFICATION NUMBER F19628-86-C-0077
	10. SOURCE OF FUNDING NUMBERS

PROGRAM ELEMENT NO.	PROJECT NO.	TASK NO.	WORK UNIT ACCESSION NO.
63701B	3201	DM	AE

11. TITLE (Include Security Classification)
Estimation of Short-Wavelength Gravity on a Dense Grid Using Digital Terrain Elevation Data

12. PERSONAL AUTHOR(S)
J.D.Goldstein, J.V.White, and R.P.Comer, W.G. Heller

13a. TYPE OF REPORT	13b. TIME COVERED	14. DATE OF REPORT (Year, Month, Day)	15. PAGE COUNT
Scientific No. 1	FROM May 86 TO May 87	1987 October 15	40

16. SUPPLEMENTARY NOTATION

17. COSATI CODES		
FIELD	GROUP	SUB-GROUP

18. SUBJECT TERMS (Continue on reverse if necessary and identify by block number)
Geodesy; Gravity; Gravity Gradiometry; Gravity Surveying, ~~GESS~~ Fast Fourier Transforms, Geodetic Surveys, (jhd)

19. ABSTRACT (Continue on reverse if necessary and identify by block number)

The precise determination of the gravity field at or near the earth's surface is required for compensating navigation/guidance systems and for testing gravity gradiometers. With conventional gravimeters it is usually impractical to measure the gravity field over an extended area at very short wavelengths (e.g., wavelengths less than 10 km). Since very short-wavelength gravitational perturbations at the surface are caused largely by near-surface mass variations in the local area, and since digital terrain elevation data (DTED) are available on dense grids (e.g. three arc second spacing) for selected regions, the very short-wavelength components of gravity can be estimated without a gravity survey by using the DTED and the assumption of constant mass density. This report presents an approach to computing the short-wavelength, terrain-induced gravity field at a prescribed rms accuracy. For a relatively flat test area in Oklahoma, the rms effect of terrain elevation on the gravity field at mean elevation for wavelengths shorter than 10 km varies between 0.6 mgal and 2.2 mgal. The largest point value of the high-frequency terrain effect is 18.0 mgal. Keywords:

20. DISTRIBUTION/AVAILABILITY OF ABSTRACT	21. ABSTRACT SECURITY CLASSIFICATION
☐ UNCLASSIFIED/UNLIMITED ☒ SAME AS RPT. ☐ DTIC USERS	Unclassified

22a. NAME OF RESPONSIBLE INDIVIDUAL	22b. TELEPHONE (Include Area Code)	22c. OFFICE SYMBOL
Capt. Vishnu Nevrekar	(617) 377-3486	LWG

DD FORM 1473, 84 MAR

83 APR edition may be used until exhausted.
All other editions are obsolete.

SECURITY CLASSIFICATION OF THIS PAGE
UNCLASSIFIED

ACKNOWLEDGMENT

The authors wish to thank Mahendra K. Mallick of The Analytic Sciences Corporation for his help in obtaining two-dimensional power spectra from along-track autoregressive model coefficients. This work was performed for the Air Force Geophysics Laboratory (Contract F19628-86-C-0077), under the sponsorship of the Defense Mapping Agency, in support of the Airborne Gravity Gradiometer System Test Program.

TABLE OF CONTENTS

LIST OF FIGURES

LIST OF TABLES

1. INTRODUCTION

Stringent new requirements to reduce gravity-induced uncertainties in inertial systems, to control Geodetic and Geophysical (G&G) factors during the test and evaluation of inertial instruments, and to achieve mobility for new classes of ballistic missile systems motivate more accurate means to measure the earth's gravity field. These requirements demand increasingly fine local gravity data, more accuracy at high spatial frequencies, and, in many cases, coverage of large areas.

In this report, high-resolution digital terrain elevation data (DTED) are used to compute the effect of terrain variations on the very high-frequency vertical gravity field in a local area (wavelengths shorter than 10 km). The terrain effect is computed with a specified root-mean-square (rms) accuracy as determined by an error covariance analysis that accounts for the finite extent of the DTED.

The terrain effect is only a portion of the total gravity disturbance, because regional, continental, and global-sized density variations deep below the earth's crust also contribute significantly. Nevertheless, at very short wavelengths the terrain effect is expected to dominate the gravity field in most areas (Ref. 1). Therefore, the high-frequency terrain effect is used as a reasonable estimate of the gravity disturbance at wavelengths shorter than 10 km.

This report describes a new analytical technique for using DTED to compute the high-frequency terrain effect on

gravity. The methodology is applicable for estimating all three components of the high-frequency gravity vector from DTED, for determining the lowest spatial frequency appropriate for the estimation, for sizing the zones of DTED coverage needed for a specified accuracy, and for applying modern vector/parallel numerical processing techniques on supercomputers. The approach described here is novel in two ways: it uses a direct quadrature approach to compute the terrain effect, and it includes systematic control of accuracy.

While, in principle, the accuracy of DTED could be approximately 1 to 3 m rms, in practice much of the data now in place are of unknown accuracy. Thus, the results presented herein, as well as widespread use of the methodology described in the sections which follow, appeal to the future. This future will be realized when DTED accuracy can confidently be known to match its current precision.

2. BACKGROUND

The problem addressed in this report is to estimate the high-frequency vertical gravity field of the earth at points on a horizontal grid. The vertical component of gravity is to be estimated at points that are uniformly spaced at three arc second intervals over a rectangular area containing several hundred thousand such points. The longest wavelengths of interest are about 10 km. Because these wavelengths are much smaller than the radius of the earth, the problem is formulated using the flat-earth approximation (i.e., the reference ellipsoid is approximated locally by a horizontal plane).

2.1 PROBLEM STATEMENT

The technical approach taken in this work is to use the local terrain effect on gravity, suitably filtered to attenuate low-frequency components, as the desired gravity estimate. This local terrain effect is defined as the gravity due to the earth's mass above a reference plane in a local geographical area that is large enough to provide a specified rms accuracy at high spatial frequencies. To compute the terrain effect, Newton's law of gravitation is used to express the vertical gravity as a volume integral over the local mass. The mass density of the earth is modeled as constant at 2.67×10^3 kg/m^3, which is the mean crustal density, and the surface of the earth is represented by DTED on a uniform grid. The DTED are expressed as heights above sea level to the nearest meter.

The terrain-effect integral is formulated as illustrated in Fig. 2.1-1, which depicts a vertical cross-section of the earth's crust. A Cartesian coordinate system is used, with variables x and y measuring position in the horizontal plane and variable z measuring height. The observation point P has coordinates (x_p,y_p,z_p); this is a generic point at which the vertical gravity is to be computed. The reference surface is at height z_0, and the earth's surface at position (x,y) has height h(x,y). The terrain effect at point P is the integral of the gravity contributions from all infinitesimal mass elements such as the one at point (x,y,z) in Fig. 2.1-1. The gravity potential at point P due to all mass elements is denoted $\phi(P)$ and is given by Newton's law:

$$\phi(P) = G \int_{-\infty}^{\infty}\int\int \frac{\rho(x,y,z)}{R_p(x_p,y_p,z_p,x,y,z)} \, dxdydz \qquad (2.1\text{-}1)$$

where G is the gravitational constant (6.672×10^{-11} $m^3\cdot kg^{-1}\cdot s^{-2}$), ρ is the mass density, which is modeled as a constant (2.67×10^3 $kg\cdot m^{-3}$), and R_p is distance from the observation point. The vertical component of the terrain effect at point P is denoted g(P) and is measured positive in the downward (negative z) direction. From potential theory, it follows that

$$g(P) = -\frac{\partial\phi(P)}{\partial z_p} \qquad (2.1\text{-}2)$$

Therefore,

$$g(P) = G\rho \int_{-\infty}^{\infty}\int dxdy \int_{z_0}^{h(x,y)} \frac{z_p - z}{R_p^3} \, dz \qquad (2.1\text{-}3)$$

G-02023

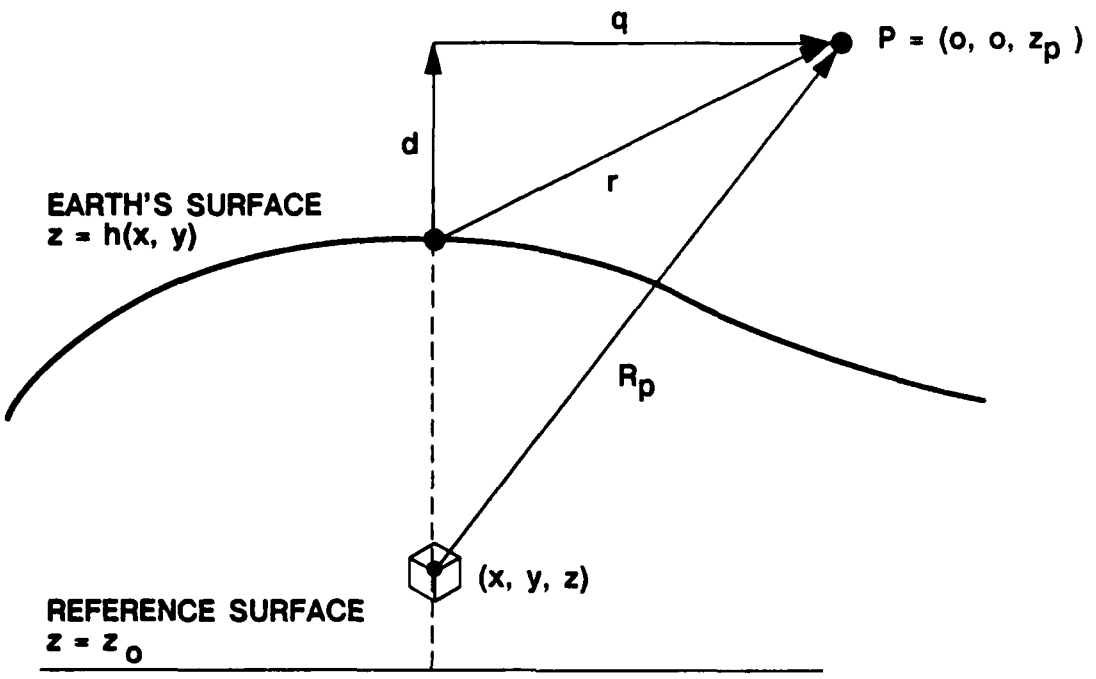

Figure 2.1-1 Vertical Cross-Section of Earth's Crust in Relation to Observation Point P

The integration with respect to z in Eq. 2.1-3 can be expressed in closed form. For mathematical convenience, this integration is performed in two steps:

$$\int_{z_0}^{h(x,y)} \frac{z_p - z}{R_p^3}\, dz = \int_{z_0}^{z_p} \frac{z_p - z}{R_p^3}\, dz + \int_{z_p}^{h(x,y)} \frac{z_p - z}{R_p^3}\, dz \qquad (2.1\text{-}4)$$

The decomposition of Eq. 2.1-4 leads to the following expression for the vertical terrain effect:

$$g(p) = 2\pi G\rho|z_p - z_0| + G\rho \iint_{-\infty}^{\infty} \left(\frac{1}{r} - \frac{1}{q}\right) dxdy \qquad (2.1\text{-}5)$$

where q and r are defined by Fig. 2.1-1 and by Eqs. 2.1-6, 2.1-7, and 2.1-8:

$$q(x_p, y_p, x, y) = \left[(x_p - x)^2 + (y_p - y)^2\right]^{\frac{1}{2}} \qquad (2.1\text{-}6)$$

$$d(z_p, x, y) = z_p - h(x, y) \qquad (2.1\text{-}7)$$

$$r = (q^2 + d^2)^{\frac{1}{2}} \qquad (2.1\text{-}8)$$

In Eq. 2.1-5, the terrain effect is expressed as the sum of two terms, which are termed the slab effect and the terrain correction. The slab effect is the first term and, analogously to a Bouguer plate, represents the vertical component of gravity due to an infinite horizontal slab of mass filling the space between the lower reference surface and the observation point. The terrain correction is the two-dimensional integral over the horizontal plane, which accounts for terrain deviations from the top of the slab.

In this analysis, all observation points have the same heights so that z_p is fixed, and the slab effect is constant. The major challenge in computing the terrain effect is the numerical evaluation of the terrain-correction integral in Eq. 2.1-5, i.e.

$$I(P) = G\rho \iint_{-\infty}^{\infty} \left(\frac{1}{r} - \frac{1}{q}\right) dxdy \qquad (2.1\text{-}9)$$

Integral I(P) must be evaluated for each grid point P at which gravity is being computed.

2.2 PREVIOUS APPROACHES

This section reviews previous approaches to the calculation of terrain corrections on a dense grid using DTED: the prism approach and two variations on the more recent Fast Fourier Transform (FFT) approach.

2.2.1 PRISM Approach

A frequently used approach to evaluating the terrain effect based on DTED is to approximate the terrain as a collection of prisms of constant mass density and then apply an analytic expression for the gravity disturbance due to each prism (e.g. Ref. 1). Flat-topped prisms are often used in which h(x,y) is assumed constant on each of a set of rectangles in the x-y plane. The formula for each prism requires the evaluation of eight logarithms and eight arctangents, along with numerous subtractions. This approach imposes several drawbacks: the high computational cost of evaluating the transcendental functions, ill-conditioning due to cancellation errors, and the introduction of spurious high frequency gravity signal due to the abrupt edges of the prisms.

A recently developed alternative is the FFT approach (Refs. 2, 3, and 4), in which the terrain-correction integral

is approximated as a sum of linear convolutions that are implemented as multiplications in the spatial frequency domain.

The key approximation in evaluating Eq. 2.1-9 is to replace

$$\frac{1}{r} - \frac{1}{q}$$

by

$$-\frac{1}{2}\frac{d^2}{q^3}$$

Note that this approximation is quite accurate for q>>d. Further discussion and application, accounting for this restriction, is presented in Section 3.2. The result is

$$I(P) \cong -\frac{1}{2} G\rho \iint_{-\infty}^{\infty} \frac{d^2}{q^3}\, dxdy \qquad (2.2\text{-}1)$$

2.2.2 FFT Approach

For the case of the classical terrain correction, in which the computation point P is on the surface of the terrain, the FFT method is developed with the simplification, $z_p = h_p$, where $h_p = h(x_p,y_p)$ and

$$d = h_p - h(x,y) \qquad (2.2\text{-}2)$$

The first term on the right side of Eq. 2.1-5 then reduces to the classical Bouguer reduction (e.g., Ref. 5). Note that for $z_p \neq h_p$ the integral in Eq. 2.2-1 fails to converge. (A simple

example of this divergence is the trivial case in which $z_p \neq 0$ and $h(x,y) = 0$.)

The next step in the FFT method is to define

$$f(x,y) = (x^2 + y^2)^{-3/2} \qquad (2.2\text{-}3)$$

so that

$$\frac{1}{q^3} \equiv f(x_p\text{-}x,\ y_p\text{-}y) \qquad (2.2\text{-}4)$$

Equation 2.2-1 may then be written as

$$I(P) \cong -\frac{1}{2}G\rho \iint_{-\infty}^{\infty} (h(x,y)\text{-}h_p)^2\ f(x_p\text{-}x, y_p\text{-}y)\ dxdy \qquad (2.2\text{-}5)$$

Expanding the squared quantity leads to a sum of linear convolutions of f with h and h^2, plus a constant term. The convolutions may be evaluated (approximately) by multiplication in the discrete spatial frequency domain with the use of a two-dimensional FFT. Clearly, one advantage of such a method is that, upon return from the frequency domain, the values of the terrain effect are available on an entire grid of points.

One troublesome problem, however, is that the integral of f over the x-y plane is divergent, which causes the Fourier transform of f to become undefined. Furthermore, expanding Eq. 2.2-5 results in a difference of infinite quantities. Nonetheless, according to Refs. 3 and 4, replacing f(0,0) by 0 in the discrete computations can lead to reasonable numerical results. In this instance, the argument is made that the integral of f over the plane can be replaced by the discrete Fourier transform of the discretized, modified f, evaluated at zero frequency. Unfortunately the process is ad hoc and universal applicability cannot be assured.

A variation, proposed in Refs. 2 and 4, is to replace f by

$$g(x,y) = (x^2 + y^2 + b^2)^{-3/2} \qquad (2.2\text{-}6)$$

where b is a nonzero constant whose dimension is length. It can be shown that

$$\iint_{-\infty}^{\infty} g(x,y)\, dxdy = 2\pi/b \qquad (2.2\text{-}7)$$

and that the Fourier transform of g exists and has a simple analytic form.

2.2.3 Modified FFT Approach

References 2 and 4 advocate choosing as small a value of the parameter b as possible. However, Ref. 6 shows that substitution of

$$(q^2 + b^2)^{1/2}$$

for

$$R_p = (q^2 + (z_p - z)^2)^{1/2} \qquad (2.2\text{-}8)$$

in the rightmost integral of Eq. 2.1-4 leads directly to the approximation

$$I(P) \cong -\frac{1}{2} G\rho \iint_{-\infty}^{\infty} (h(x,y)-z_p)^2\, g(x_p-x,\, y_p-y)\, dxdy \qquad (2.2\text{-}9)$$

instead of Eq. 2.2-5. Equation 2.2-9 shows that b^2 should be a kind of average of $(z_p-z)^2$ and should not be arbitrarily chosen to be as small as possible. Note also that, in the formulation of Eq. 2.2-9, the FFT approach is no longer limited to computation points on the terrain surface; z_p in Eq. 2.2-9 need not equal h_p, and I(P) can be readily evaluated in terms of the convolution of g with h and h^2.

However, even with the improvements afforded by Eqs. 2.2-6 and 2.2-9, an approximation is involved in the FFT method, which (like the prism representation) may incur high-frequency errors and edge-effect problems. Therefore, instead of applying one of the conventional methods, the preferred technique pioneered herein is a completely alternative approach to the computation of terrain corrections. It is simple in principle yet appears to have been overlooked previously because of the unavailability of modern parallel processing resources: direct quadrature of Eq. 2.1-9.

3. ANALYTICAL APPROACH

This chapter discusses several issues related to the numerical integration in Eq. 2.1-9:

- Avoiding cancellation errors in the evaluation of the integrand using finite precision arithmetic.
- Accounting for the singularity at the origin in Eq. 2.1-9.
- Determining the extent of the integration domain needed to achieve the required accuracy for short-wavelength gravity.

The next three sections discuss each of these issues.

3.1 AVOIDING CANCELLATION ERRORS

Equation 2.1-9 is unsuited for numerical computations, because the integrand is the difference of two terms nearly equal to each other. When finite precision floating point arithmetic is used, the mantissas of both terms almost coincide, and the difference between the two numbers is reflected only in their least significant bits. The relative accuracy with which the difference can be computed is equal to that fraction of the mantissa where the two terms differ.

The errors that arise from computing the difference between two nearly equal numbers are usually termed cancellation errors. To avoid them, Eq. 2.1-9 can be written as

$$I(P) = G\rho \iint_{-\infty}^{\infty} \frac{q-r}{qr}.\frac{q+r}{r+q}\, dxdy = -G\rho \iint_{-\infty}^{\infty} \frac{r^2 - q^2}{qr(r+q)}\, dxdy \qquad (3.1\text{-}1)$$

which reduces to

$$I(P) = -G\rho \iint_{-\infty}^{\infty} \frac{d^2}{qr(r+q)}\, dxdy \qquad (3.1\text{-}2)$$

The integrand in Eq. 3.1-2, although more complicated than the integrand of Eq. 2.1-9, is now much better suited for numerical computations.

3.2 ACCOUNTING FOR THE SINGULARITY AT THE COMPUTATION POINT

The integrand in Eq. 3.1-2 is singular at the computation point P, where $(x,y) = (x_p,y_p)$. By changing to polar coordinates centered on the computation point, it can be seen that the singularity at the computation point is integrable. Thus, from a purely theoretical point of view, the singularity presents no problem. However, the limiting process needed to integrate the singularity requires the knowledge of $h(x,y)$ over a continuum in the neighborhood of (x_p,y_p). Since, in practice, the terrain elevation, $h(x,y)$, is known only on a discrete set of points, the behavior of $h(x,y)$ near (x_p,y_p) has to be inferred from the values at (x_p,y_p) and at points nearby.

A planar approximation to the terrain elevation is used in the neighborhood of the origin; that is

$$h(x,y) = ax + by + c \qquad (3.2\text{-}1)$$

with the parameters a, b, and c chosen to make Eq. 3.2-1 the best (least-squares) planar* fit to the terrain elevation directly under the computation point and the four nearest grid points. Using the notation of Fig. 3.2-1, the values of the parameters are

G-02024

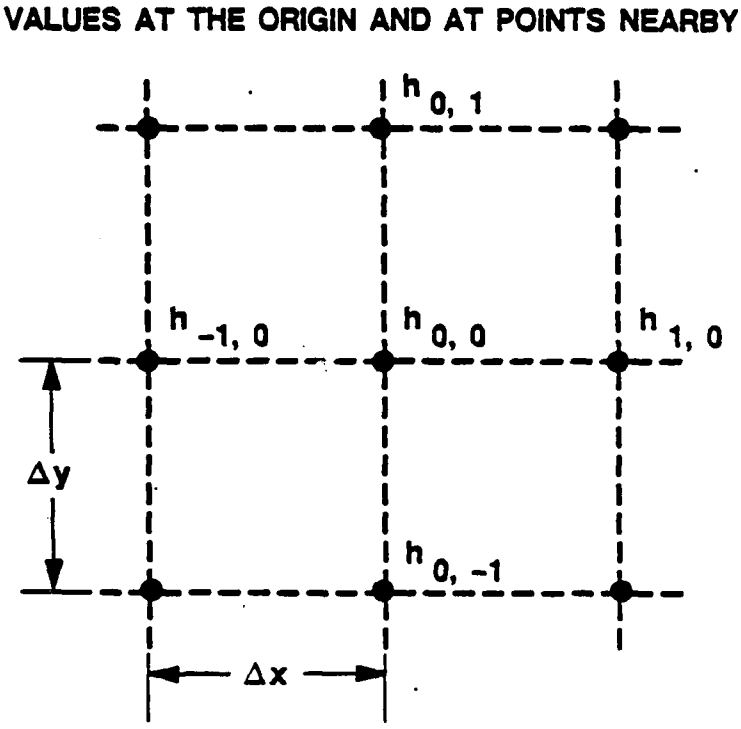

Figure 3.2-1 Grid Points Used to Approximate h(x,y) near the Origin

*Note that, if appropriate, there is no reason why a higher order surface could not be used.

$$a = \frac{h_{1,0} - h_{-1,0}}{2(\Delta x)} \qquad (3.2\text{-}2)$$

$$b = \frac{h_{0,1} - h_{0,-1}}{2(\Delta y)} \qquad (3.2\text{-}3)$$

and

$$c = \frac{h_{0,0} + h_{1,0} + h_{0,1} + h_{-1,0} + h_{0,-1}}{5} \qquad (3.2\text{-}4)$$

MACSYMA* (Ref. 7) was used to obtain the integral of Eq. 3.1-2 after substituting the planar approximation for h(x,y) in the integrand. The integration was done by expanding the integrand as a Taylor series in the planar slope, and then integrating the series term by term. Ideally, one would perform the integration over a rectangle of area $A = (2\Delta x)\cdot(2\Delta y)$ centered at the computation point. This is not tractable in practice, however, so a circle of radius R_o, chosen so that $\pi R_o^2 = A$, is used instead. (For the DTED used in this study, $R_o = 95$ m.) Some numerical experiments were conducted to determine how many terms in the series were needed to obtain an accuracy of 0.01 mgal. The results showed that terms up to degree 2 are sufficient, given the ranges of terrain elevations and slopes in the DTED used for this study. The formula used to compute the contribution to the terrain correction from the area directly under the computation point is

$$I_o(P) = 2\pi G\rho \left\{ (R_o^2 + e^2)^{\frac{1}{2}} - R_o - e + \left(e - \frac{R_o^4 + 6e^2R_o^2 + 4e^4}{4(R_o^2 + e^2)^{\frac{1}{2}}} \right) s^2 \right\} \qquad (3.2\text{-}5)$$

*MACSYMA is a trademark of Symbolics Inc.

where $s = (a^2 + b^2)^{\frac{1}{2}}$ is the slope of the planar approximation and $e = |z_p - c|$ is the vertical distance from the point P to the planar approximation.

3.3 EXTENT OF THE INTEGRATION DOMAIN

The integration in Eq. 3.1-2 cannot be performed numerically over the entire x-y plane. The domain of integration has to be truncated, thereby introducing errors in the computation. Ideally, the truncation errors should be at least as small as those caused by discretization effects. Thus it is appropriate to relate the size of the integration area explicitly to the desired accuracy of the numerical integration. Insight into the dimensions of the required region of integration is gained by noting that short-wavelength components of gravity are due to nearby masses. Therefore, the integration in Eq. 3.1-2 needs to extend only far enough to account accurately for these wavelengths.

The error made by limiting the integration in Eq. 3.1-2 to a circle of radius R centered at the computation point is

$$\delta I(x_p, y_p, z_p) = -G\rho \iint_{q>R} \frac{d^2}{qr(r+q)}\, dxdy \qquad (3.3\text{-}1)$$

In the geographical area of interest, the values of d are of the order of a few hundreds of meters. Since R is expected to be of the order of ten or twenty kilometers, the approximation

$r \approx q$ is quite accurate for $q>R$, and Eq. 3.3-1 simplifies to

$$\delta I(x_p,y_p,z_p) = \frac{-G\rho}{2} \iint_{q>R} \frac{d^2}{q^3}\, dxdy \qquad (3.3\text{-}2)$$

Furthermore, because it is always true that $r \geq q$, the integrand of Eq. 3.3-1 is less than or equal to the integrand of Eq. 3.3-2; therefore, Eq. 3.3-2 provides an upper bound on δI.

Note that the integral in Eq. 3.3-2 is a convolution, which is conveniently rewritten as

$$\delta I(x_p,y_p,z_p) = \frac{-G\rho}{2} \iint_{A} \frac{d^2(z_p,x,y)}{[(x_p-x)^2 + (y_p-y)^2]^{3/2}}\, dxdy \qquad (3.3\text{-}3)$$

where the integration domain is

$$A = \{ (x,y) \mid [(x_p-x)^2 + (y_p-y)^2]^{\frac{1}{2}} > R \} \qquad (3.3\text{-}4)$$

Hence, the truncation errors can be obtained as the convolution of the squared height difference, $d^2(z_p,x,y)$, and the function

$$T(x,y) = \begin{cases} 0 & \text{if } q(x_p,y_p,x,y)<R \\ \dfrac{-G\rho}{2q^3} & \text{if } q(x_p,y_p,x,y)>R \end{cases} \qquad (3.3\text{-}5)$$

If the terrain elevation is modeled as a stationary random process, then the squared elevation is also stationary, and it follows from Eq. 3.3-3 that the truncation-error power spectrum is

$$\Phi_{\delta I} = |\hat{T}|^2 \Phi_s \qquad (3.3\text{-}6)$$

where Φ_s is the power spectrum of the squared elevation difference, $s(x,y) = d^2(x,y)$, and $\hat{T}$ is the Fourier transform of T defined by

$$\hat{T}(f_1,f_2) = \int_{-\infty}^{\infty}\int T(x,y)\, e^{-i2\pi(f_1x+f_2y)}\, dxdy \qquad (3.3\text{-}7)$$

This Fourier transform can be expressed as

$$\hat{T}(f_1,f_2) = \frac{-\pi G\rho}{R}\, Q(2\pi Rf) \qquad (3.3\text{-}8)$$

with $f = (f_1^2 + f_2^2)^{\frac{1}{2}}$. The function Q is computed numerically in terms of J_o, the Bessel function of the first kind, order zero

$$Q(x) = \int_x^{\infty} \frac{J_o(u)}{u^2}\, du \qquad (3.3\text{-}9)$$

For any given choice of R, Eq. 3.3-6 provides a decomposition of the truncation errors into their spectral components. The variance of the errors at wavelengths shorter than 10 km, σ_0^2, is obtained by integrating the spectral density $\Phi_{\delta I}$ over radial frequencies higher than f_o = 1/10 cyc/km; that is,

$$\sigma_o^2 = \iint_{f>f_o} |\hat{T}|^2 \Phi_s\, df_1 df_2 \qquad (3.3\text{-}10)$$

Note that the error variance σ_o^2 depends on the choice of R through the function $\hat{T}$ (see Eq. 3.3-8). To determine how large R should be, a table of values of σ_o^2 as a function of R is constructed. The integration radius, R, is then chosen as that value in the table for which the error variance is within the required limits. Before such a table can be constructed, however, the spectrum ϕ_s in Eq. 3.3-10 must be evaluated.

In the current study, the spectral density of the squared elevation differences, Φ_s, was estimated using the DTED in the study area. Various east-west and north-south tracks were selected in the area, and the values of $s = d^2$ were computed from the terrain elevation along each track. One-dimensional power spectra were then obtained by fitting autoregressive models to d^2-m (where m is the sample mean along the track) using the "covariance method" (*Refs. 8-10*). The estimated along-track spectra tended to cluster into two groups: one for the northern, and another for the southern region of the study area.

This clustering reflects differences in ruggedness which are visually apparent from a graphical display of the terrain elevation (Fig. 3.3-1). In the range of frequencies of interest, the spectrum for the northern tracks is uniformly higher than that for the southern tracks. This behavior corresponds to the more rugged terrain in the northern region of the area being analyzed.

It can be seen from Eq. 3.3-10 that the larger Φ_s, the larger the error variance of the truncation errors, and the more stringent the requirement on the value of R. Therefore, the model for the northern region was used in the determination of the value of R.

Figure 3.3-1 Three-Dimensional Rendering of DTED

The function Φ_s needed in Eq. 3.3-10 is the <u>two-dimensional</u> power spectrum of the squared terrain differences. Modeling ϕ_s as isotropic, it can then be computed from the corresponding one-dimensional along-track spectrum using the Abel transform (Refs. 11 and 12). The result is a spectrum, $\Phi(f)$, that is a function of radial frequency only:

$$\phi_s(f_1,f_2) = \phi\ (f_1^2+f_2^2)^{1/2} \qquad (3.3\text{-}11)$$

Since the function $\hat{T}$ is also only a function of f (see Eq. 3.3-8), Eq. 3.3-10 simplifies to

$$\sigma_o^2 = 2\pi \int_{f_o}^{\infty} |\hat{T}(f)|^2 \phi(f)\ f\ df \qquad (3.3\text{-}12)$$

Equation 3.3-12 was used to compute the data in Table 3.3-1, which lists different values of R and the corresponding rms truncation error σ_o. For example, if the vertical terrain effect is computed for wavelenghts shorter than 10 km using DTED within a 3-km radius of the computation point, then Table 3.3-1 indicates that the rms error due to the finite amount of DTED is 0.0081 mgal.

TABLE 3.3-1
RMS TRUNCATION ERROR CAUSED BY
FINITE EXTENT OF DTED

RADIUS R (km)	RMS ERROR* δ (mgal)
1	0.083
2	0.013
3	0.0081
4	0.0054
5	0.0031
6	0.0017
7	0.0012
8	0.0010
9	0.00078
10	0.00054
20	0.00010

*For wavelengths shorter than 10 km.

4. DISCUSSION

4.1 DATA

The Defense Mapping Agency provided the DTED used for this analysis. These DTED cover a region that includes the Clinton-Sherman Airport in Oklahoma and consist of terrain heights above sea level on a uniform latitude-longitude grid having a point spacing of three seconds of arc, with the heights expressed to the nearest meter. The object of the present analysis is to estimate the high-frequency vertical gravity field in a 512 by 512-point subregion that includes a topographic feature called Baker Peak. It is desired to compute the local terrain effect at each grid point in this subregion with an rms accuracy of 0.01 mgal for wavelengths shorter than 10 km. According to Table 3.3-1, to achieve this accuracy, DTED are needed within a 3-km radius of each computation point. Therefore, the numerical quadrature of the terrain-correction integral was performed over a square area spanning 9π km^2 and centered on each computation point.

In Fig. 3.3-1, the DTED are rendered as a three-dimensional surface, with the vertical scale greatly magnified for visual clarity. Although the northern (upper) half of Fig. 3.3-1 looks mountainous, the DTED actually fall in a range from approximately 200 m to 700 m above sea level. The region depicted in Fig. 3.3-1 extends 57 km east-west and 65 km north-south. The average distance between grid points is 76.5 m east-west and 92.7 m north-south.

4.2 COMPUTATIONAL APPROACH

To generate estimates of high-frequency gravity on a dense grid, the local terrain effect is first computed at each grid point. Then the resulting two-dimensional (2-D) field is filtered with a 2-D high-pass filter. Computing the terrain effect is the major data processing effort, because the terrain effect integral in Eq. 3.1-2 must be evaluated at each point on the grid. In particular, for the 512 by 512-point grid used in this paper, the terrain effect integral is evaluated numerically 262,144 times. Each of these numerical quadratures involves the following three steps: (1) the integrand is evaluated at the 4,189 grid points within the 54 by 71 point domain of integration; (2) at each of these points, the value of the integrand is multiplied by a weighting factor, w_k, determined by the numerical quadrature rule; and (3) the resulting products are summed and scaled by the grid-spacing factor $4 \cdot \Delta x \cdot \Delta y$.

The computational approach described here is appropriate for computers having a Cray-type architecture for parallel vector computation, e.g., the Alliant FX/8 minisupercomputer used in this study. On such machines, arithmetic operations applied uniformly to large arrays can be performed much more rapidly than an equivalent number of scalar calculations. Therefore, to achieve high computational speed, the computations are expressed as uniform operations on large arrays.

The terrain effect integral is evaluated using the following nine-point numerical quadrature formula (Ref. 13):

$$\iint_S f(x,y)\, dxdy = 4 \cdot \Delta x \cdot \Delta y \sum_{k=1}^{9} f(x_k, y_k) w_k + 0(A^2) \quad (4.2\text{-}1)$$

where the domain S is the $2 \cdot \Delta x$ by $2 \cdot \Delta y$ rectangle ($-\Delta x \leq x \leq \Delta x$, $-\Delta y \leq y \leq \Delta y$) of area $A = 4 \cdot \Delta x \cdot \Delta y$. As depicted in Fig. 4.2-1, the knot points (x_k, y_k) are on a rectangular grid with spacings Δx and Δy in the x and y directions, respectively, and the weights, $4w_k$, are the outer product of the weights (1/6, 2/3, 1/6) for the three-term Simpson's formula. The error of this quadrature rule is asymptotically of order A^2 as A goes to zero.

According to the error analysis in Section 3.3, the domain of the terrain-effect integral can be truncated to a rectangular area centered on the computation point P as depicted schematically in Fig. 4.2-2. This domain contains $(2M+1) \cdot (2N+1)$ DTED grid points. Applying Eq. 4.2-1 to each adjacent 9-point rectangle and summing the results over the domain depicted in Fig. 4.2-2 will yield the desired numerical quadrature, except for the center region containing point P, which is omitted from this quadrature. The center region is handled separately as discussed in Section 3.2. To achieve high speed on a parallel-vector computer, the multiple applications of Eq. 4.2-1 should be formulated as a single large array operation. This is done by developing a single (2M+1) by (2N+1)-point (large-scale) quardrature formula that is equivalent to multiple applications of the 9-point formula. The resulting weight pattern over the interior of the domain is depicted in Fig. 4.2-2. (The weights along the outer edges and the weights along the omitted inner region containing point P are different from the interior pattern depicted in Fig. 4.2-1)

After evaluating the terrain correction integral on the 512 by 512 grid, the final step in estimating high-frequency gravity is to filter-out the low-frequency components of the computed terrain effects. A 2-D finite-impulse-response high-pass filter is used for this purpose. The output of the filter, y(j,k), is the value of the input datum, x(j,k), minus the

G-02025

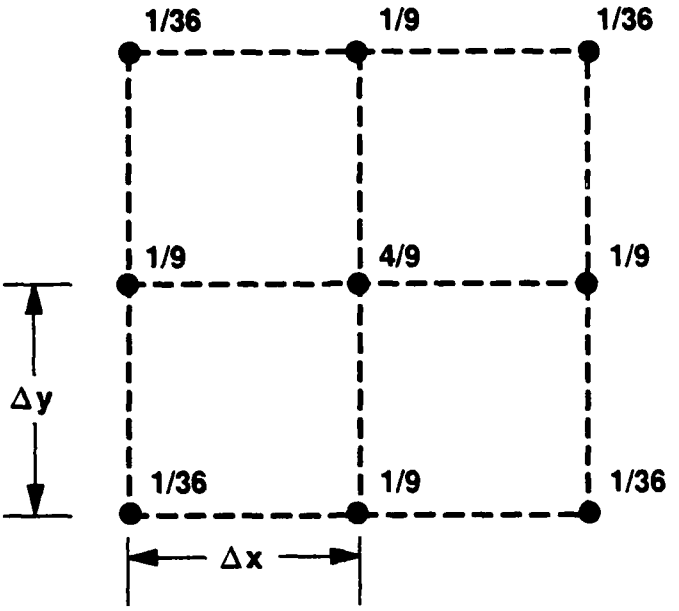

Figure 4.2-1 Domain and Weights W_k of Nine-Point Quadrature Formula

G-02021

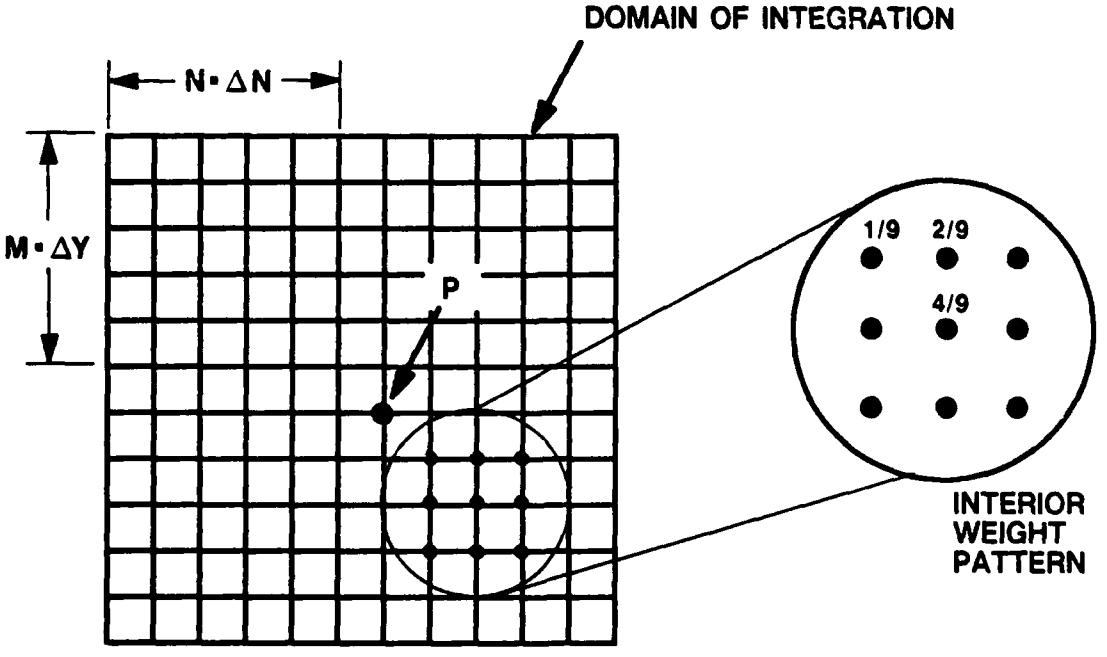

Figure 4.2-2 Schematic Representation of Integration Domain for Point and Interior Weight Pattern for Large-Scale Numerical Quadrature

average of x(j,k) over a $(2N_x+1)$ by $(2N_y+1)$-point rectangle centered on point (j,k):

$$y(j,k) = \sum_{m=-N_y}^{N_y} \sum_{n=-N_x}^{N_x} H(m,n)x(j-m,k-n) \qquad (4.2\text{-}2)$$

$$H(0,0) = 1 - (2N_x+1)^{-1}(2N_y+1)^{-1} \qquad (4.2\text{-}3)$$

$$H(m,n) = -(2N_x+1)^{-1}(2N_y+1)^{-1} \qquad (4.2\text{-}4)$$

The transfer function of this filter, $\bar{H}(F_y,F_x)$, is expressed using the normalized frequencies, $F_x = \Delta x f_x$ and $F_y = \Delta y f_y$, where F_x and F_y range in absolute value from 0 to 1/2:

$$\bar{H}(F_y,F_x) = 1 - \bar{H}_y(F_y)\bar{H}_x(F_x) \qquad (4.2\text{-}5)$$

$$\bar{H}_x(F_x) = \mathrm{sinc}[(2N_x+1)F_x]/\mathrm{sinc}(F_x) \qquad (4.2\text{-}6)$$

$$\bar{H}_y(F_y) = \mathrm{sinc}[(2N_y+1)F_y]/\mathrm{sinc}(F_y) \qquad (4.2\text{-}7)$$

$$\mathrm{sinc}(0) = 1 \qquad (4.2\text{-}8)$$

$$\mathrm{sinc}(x) = \sin(\pi x)/(\pi x) \qquad \text{for } x \neq 0 \qquad (4.2\text{-}9)$$

The frequency response of this filter (i.e., the squared magnitude of the transfer function) is plotted in Fig. 4.2-3 for $F_y = 0$ as a function of the dimensionless east frequency $w_x f_x$, where w_x is the length of the filter impulse response in the x direction, and f_x is the frequency expressed in cycles per unit length (i.e., $w_x f_x = (2N_x+1)\Delta x f_x = (2N_x+1)F_x$). The low-frequency limit of this filter is defined as the frequency for which the

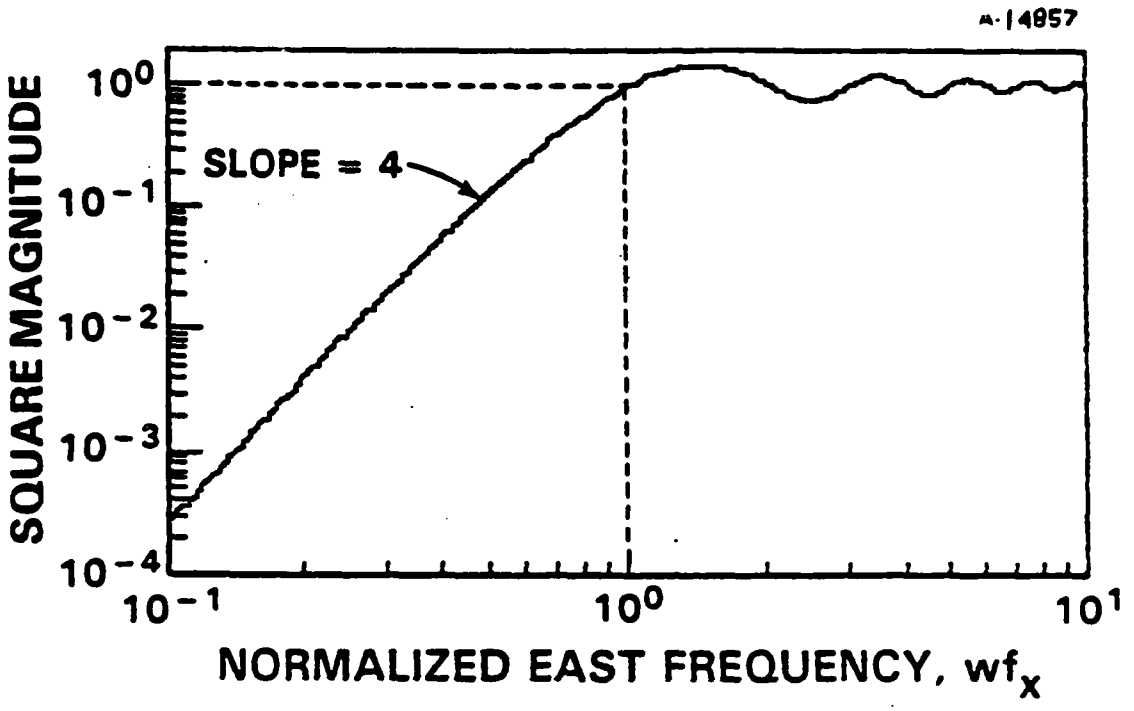

Figure 4.2-3 Frequency Response of High-Pass Filter for East Frequencies ($f_y = 0$)

squared mangitude of the transfer function is 1/2. It can be shown that a specified low-frequency limit, f_0, is achieved for both north and east frequencies by selecting the filter parameters N_x and N_y to satisfy the following formulas, in which int(x) denotes the value of x rounded to the nearest integer:

$$N_x = \text{int}\left(\frac{0.76}{2\Delta x f_0} - \frac{1}{2}\right) \qquad (4.2\text{-}10)$$

$$N_y = \text{int}\left(\frac{0.76}{2\Delta y f_0} - \frac{1}{2}\right) \qquad (4.2\text{-}11)$$

4.3 RESULTS

The results of using the computational approach described in Section 4.2 are depicted in Fig. 4.3-1, which is a three-dimensional rendering of the estimated vertical gravity field for wavelengths shorter than 10 km. The elevation, z_p, is equal to the average of the DTED over the analyzed area. The northern (upper) region in Fig. 4.3-1, which contains 1.2×10^5 grid points, has an rms value that is five times the

Figure 4.3-1 Three-Dimensional Rendering of Estimated Vertical Gravity for Wavelengths Shorter than 10 km

4.3 RESULTS

The results of using the computational approach described in Section 4.2 are depicted in Fig. 4.3-1, which is a three-dimensional rendering of the estimated vertical gravity field for wavelengths shorter than 10 km. The elevation, z_p, is equal to the average of the DTED over the analyzed area. The northern (upper) region in Fig. 4.3-1, which contains 1.2×10^5 grid points, has an rms value that is five times the

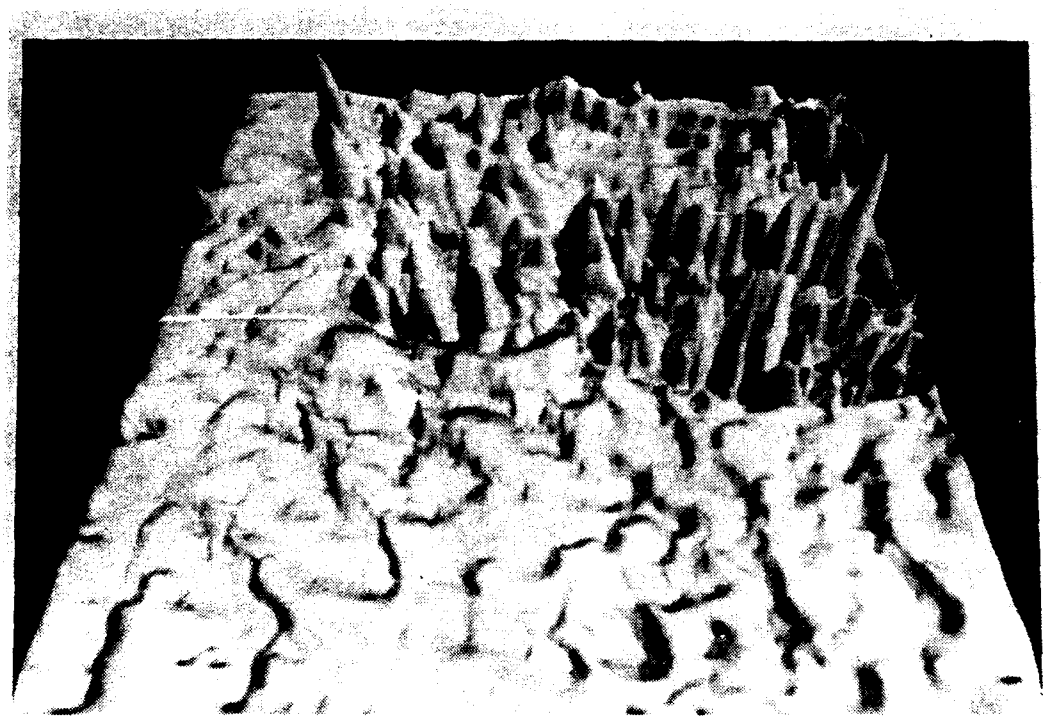

Figure 4.3-1 Three-Dimensional Rendering of Estimated Vertical Gravity for Wavelengths Shorter than 10 km

rms field in the southern region, which contains 1.2×10^4 grid points. Key statistics for the estimated gravity fields in these two regions are compared in Table 4.3-1.

The error analysis in Section 3.3 indicates that the high-frequency vertical terrain effect was computed with an rms error of 0.0081 mgal, because the DTED data extended 3 km from each computation point. To verify this small error, the terrain effects were recomputed using DTED data within a 10-km radius of each computation point. According to Table 4.3-1, the rms error of this computation is 0.00054 mgal. This more accurate field calculation was subtracted from the original results, and the rms difference was consistent with the theoretical rms error of 0.0081 mgal given in Table 3.3-1 for R = 3 km.

An additional error analysis, not presented here, shows that a much larger extent of DTED (i.e., larger R) is required to achieve similar accuracies when computing the deflections of the vertical contributed by the terrain effect. For example, an rms accuracy of 0.15 mgal requires DTED within a 10-km radius of each computation point.

TABLE 4.3-1

STATISTICS OF ESTIMATED GRAVITY FIELDS
FOR WAVELENGTHS SHORTER THAN 10 km

STATISTIC	GRAVITY IN NORTHERN REGION (mgal)	GRAVITY IN SOUTHERN REGION (mgal)
MAXIMUM	18.0	1.5
MINIMUM	-6.8	-2.2
STD. DEV.	3.0	0.6
NO. POINTS	1.2×10^5	1.2×10^4

4.4 SUMMARY AND APPROPRIATE NEXT STEP

The formulation developed in this report surmounts certain mathematical difficulties formerly associated with calculating that portion of the gravity field which is induced by visible terrain. It also uses to advantage modern parallel-processing computer architectures to optimize calculations which would be arduous or impractical if performed in scalar sequential fashion. A statistical error analysis provides the means to control accuracy. The approach is applied to digital terrain elevation data from the Clinton-Sherman test range to develop both a set of terrain-effect gravity values and an understanding of the accuracy with which the field can be determined.

The accuracy uncertainty associated with the DTED motivates further efforts to understand and quantify the data errors. Is there a frequency range over which the accuracy does approach its precision? Can the errors be predicted? Can they be modeled? Resolution of these issues could provide the impetus for turning DMA's DTED base into a very useful tool for supplementing gravity data needed to support DoD weapon systems programs.

REFERENCES

1. Forsberg, R., and Tscherning, C.C., "The Use of Height Data in Gravity Field Approximation by Collocation", Journal of Geophysical Research, Vol. 56, No. B9, pp. 7843-7854, Sept. 10, 1981.

2. Forsberg, R., "A Study of Terrain Reductions, Density Anomalies and Geophysical Inversion Methods in Gravity Field Modelling", Air Force Geophysics Laboratory Report AFGL-TR-84-0174, April, 1984., ADA150788

3. Forsberg, R., "Gravity Field Terrain Effect Computations by FFT", Bulletin Geodesique, Vol. 59, pp. 342-360, 1985.

4. Sideris, M.G., "A Fast Fourier Transform Method for Computing Terrain Corrections", Manuscripta Geodaetica, Vol. 10, pp. 66-73, 1985.

5. Heiskanen, W.A., and Moritz, H., Physical Geodesy, W.H. Freeman and Company, San Francisco, 1967.

6. Comer, R.P., "Terrain Correction via FFT: A New Derivation" (abstract), Eos, Transactions of the American Geophysical Union, Vol. 67, No. 16, p. 260, April 1986.

7. Symbolics Inc., "VAX UNIX MACSYMA™ Reference Manual Version 11," Cambridge, MA, Nov. 1985.

8. Gray, A.H., and Markel, J.D., "Linear Prediction Analysis Programs (AUTO-COVAR)," in Programs for Digital Signal Processing, Digital Processing Committee, IEEE Acoustics, Speech, and Signal Processing, Eds., IEEE Press, New York, pp. 4.1-1-4, 1-7, 1979.

9. Kay, S.M., and Marple Jr., S.L., "Spectrum Analysis - A Modern Perspective," Proceedings of the IEEE, pp. 1380-1419, Nov. 1981.

10. Brammer, R.F., Pass, R.P., and White, J.V., "Bathymetric and Oceanographic Applications of Kalman Filtering Techniques," IEEE Transactions on Automatic Control, pp. 363-371, March 1983.

REFERENCES (Continued)

11. Mook, D.R., "An Algorithm for the Numerical Evaluation of the Hankel and Abel Transforms," IEEE Transactions on Acoustics, Speech, and Signal Processing, pp. 979-985, August, 1983.

12. Hansen, E.W., and Law, P.L., "Recursive Methods for Computing the Abel Transform and Its Inverse," Journal of the Optical Society of America, pp. 510-520, April 1985.

13. Abramowitz, M, and Stegun, I.A., (Editors), Handbook of Mathematical Functions, National Bureau of Standards, Formula 25.4.62, p.892, June 1964.